Theory of the Energy Levels and Precise Two–Photon Spectroscopy of Atomic Hydrogen and Deuterium [1]

K. Pachucki, [2] D. Leibfried, M. Weitz, A. Huber, W. König, and T.W. Hänsch

Max–Planck–Institut für Quantenoptik
Hans-Kopfermann-Straße 1
D-85748 Garching, Germany

Abstract

In last years a significant progress has been achieved both in the experimental technique and the theoretical methods for the determination of the energy levels of simple hydrogenic systems. We review recent two-photon spectroscopic measurements performed in Garching and the relevant theoretical predictions for the hydrogen energy levels. A good agreement is achieved when all theoretical contributions are included, showing the importance of recently calculated higher order corrections.

1 Introduction

The hydrogen atom is one of the basic systems in atomic physics. As the simplest of stable atoms it permits unique confrontation between fundamental experiments and theory. Spectroscopy of hydrogen has played a central role in the development of quantum mechanics and atomic physics. The interpretation of the regular visible Balmer spectrum of hydrogen has inspired several conceptual breakthroughs, from Bohr and the old quantum physics to the theories of Sommerfeld, de Broglie, Schrödinger and Dirac to the discovery of the Lamb shift and the development of modern quantum electrodynamics (QED). Today, the comparison of experimental results with theoretical predictions give a test of quantum electrodynamics, and also allows for a precise determination of physical constants. The recent progress in high resolution two-photon spectroscopy of atomic hydrogen and deuterium has also stimulated further improvements in the theoretical predictions for the Lamb shift.

In this report we describe spectroscopic experiments on atomic hydrogen developed in Garching in the last few years, and present the results of improved calculations of the higher order corrections to the hydrogen Lamb shift. We will review three experiments, a precise frequency comparison of the 1S-2S and 2S-4S transitions [2], the first direct measurement of the 1S-2S isotope shift between hydrogen and deuterium [3] and finally a determination of the absolute 1S-2S transition frequency [1]. The measurement of the frequency difference of 1S-2S and 2S-4S transition:

$$\Delta E = E(4S-2S) - \frac{1}{4}E(2S-1S) \tag{1}$$

allows the determination of the 1S Lamb shift and should ultimately become one of the most precise QED tests.

On the theoretical side, one needs an accurate description of the energy levels over the range of 12 orders of magnitude to compare the theoretical results with the experimental ones. There are many

[1] reprinted under permission from Journal of Physics B

[2] present address: Institute of Theoretical Physics, Warsaw University, Hoża 69, 00-681 Warsaw, Poland.

corrections to the Dirac energies that contribute at this precision level, namely one- and two-loop QED corrections, pure and radiative recoil corrections due to the finite nuclear mass, a correction for the finite nuclear volume and even the nuclear polarizability (for deuterium). The evaluation of these corrections is a highly nontrivial task. It involves the handling of thousands of terms, which can only be managed by computer algebraic programs. Most of them require a careful treatment due to specific cancelations of ultraviolet and infrared divergences. Additionally, different corrections require different treatments. For example in the evaluation of recoil corrections the hydrogen atom has to be considered as a two body system, while for the electron self–energy corrections the proton is treated as a static source of the Coulomb field. Thus for every correction a specific method for its evaluation has to be developed. There are also some contributions that are not purely QED effects, for instance due to the finite nuclear charge radius. The proton charge radius has been measured in electron scattering experiments, however the corresponding measurement uncertainty is now the most limiting factor in QED tests on the hydrogen atom.
In section 2 we briefly describe the laser spectrometers that are used to observe the 1S-2S and the 2S-4S transition. Also the frequency chain that links the 1S-2S transition frequency to the cesium atomic clock is explained. We then review our recent experimental results. Section 3 gives a description of the theoretical methods for the calculation of hydrogen energy levels, together with the most recent results for the different contributions. Section 4 the theoretical values of the quantities measured in our experiments are given.

2 Two–photon spectroscopy on an atomic beam of hydrogen

Doppler-free two-photon spectroscopy allows for the resolution of transitions with small natural decay-width. The atoms absorb two collinear counter propagating photons. In the atomic reference frame the co-propagating photon is shifted to the red, the counter-propagating to the violet. The transition rate depends on the sum of these two frequencies, therefore the linear term in the Doppler shift cancels out and there remains only a small residual purely relativistic Doppler effect of order $(\frac{v}{c})^2$, which leads to inhomogeneous broadening of the resonance. The 1S–2S transition in hydrogen has a natural line-width of only 1.3 Hz and can currently be resolved to 3 parts in 10^{12}. For the 2S-4S transition the natural line-width of 690 kHz is the factor that limits our experimental resolution.

2.1 The 1S-2S spectrometer

To drive the 1S-2S two photon transition [5], we start from a stable dye laser at 486 nm, that is frequency-stabilized to a passive Fabry-Perot resonator (finesse 57000, resonance width 5 kHz) and can be tuned relative to the fixed longitudinal resonator modes with the help of an acousto-optic modulator (AOM). The absolute stability was measured to be 1.5 kHz in 1 s average time. The output of the dye laser is frequency doubled in a BBO crystal within an external enhancement cavity, as shown in Fig. 1. The resulting uv radiation at 243 nm is then coupled into a standing wave resonator inside a vacuum chamber. Atomic hydrogen is produced in a radio-frequency gas discharge and guided to a liquid nitrogen cooled nozzle by a teflon tube. Due to inelastic collisions the atoms thermalize with the nozzle walls. The cold ground state atoms emerge from the nozzle and form an atomic beam. Atoms are excited into the metastable 2S state along a 11.5 cm interaction region by Doppler-free two-photon transitions (see Fig. 1). At the end of the interaction region a small electric field is applied to mix the 2S state with the quickly decaying 2P state inside the Lyman-α detector, and the resulting fluorescence photons are counted by a solar blind photomultiplier. The 1S-2S line shape is determined by the time of flight broadening and the second order Doppler effect, that red-shifts the transition frequency of moving atoms. Due to the interaction with the liquid nitrogen cooled nozzle, the hydrogen atoms reduce their average velocity to 1300 m/s. At T=80 K the 1S-2S two photon resonance can be observed with a line-width of 32 kHz [5].

2.2 The 2S-4S spectrometer

To drive the 2S-4S transition [2] we use radiation at 972 nm, provided by a stable Ti:sapphire laser (absolute frequency stability 10-15 kHz in 1s average time). The hydrogen atoms are dissociated in a microwave gas discharge and excited to the metastable 2S state by electron impact. The metastable atoms fly collinearly to a standing wave of 972 nm light, that is formed by a linear resonator. If they are excited to the 4S state, they quickly decay mainly to the 1S ground state via the 3P and 2P states. The transition is detected in two ways. At the end of the excitation region, the flux of

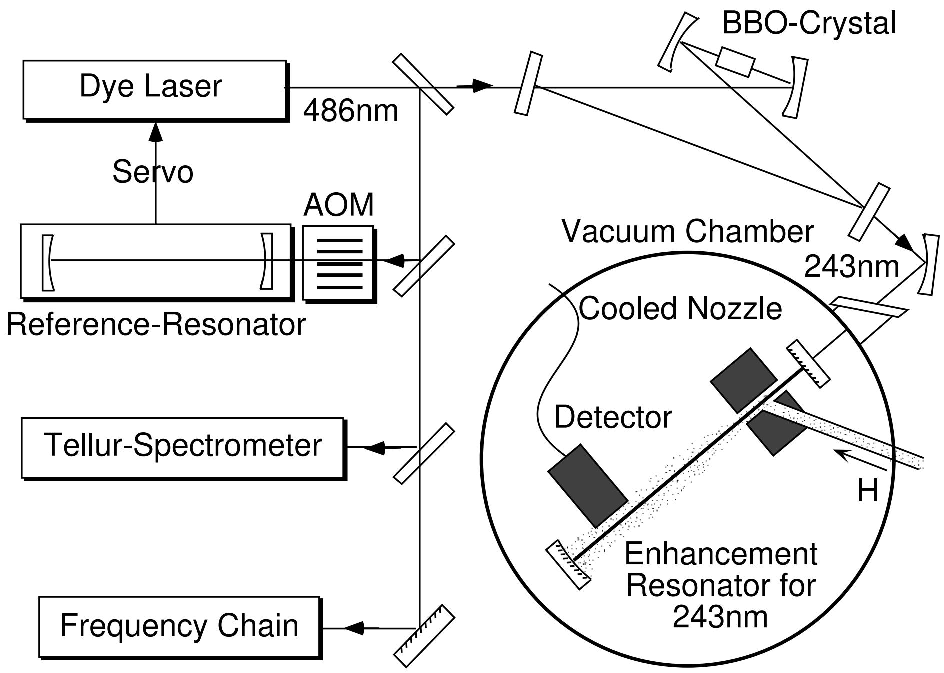

Figure 1: Setup of the hydrogen 1S-2S spectrometer.

metastable atoms is observed. On resonance the flux of 2S atoms decreases. Simultaneously, the 4S-2P fluorescence is detected along the atomic beam path. The observed 2S-4S lineshapes have a width of about 1 MHz, which is slightly above the natural line-width due to power broadening and the spatially inhomogeneous AC-Stark shift [2].

2.3 Absolute frequency measurement of the 1S-2S transition

To perform the frequency measurement [1] of the hydrogen 1S-2S energy separation, we take advantage of the near coincidence between the 28th harmonic of the methane stabilized helium neon laser (HeNe/CH_4) at 88 THz and the 1S-2S frequency. Our transportable HeNe/CH_4 standard has been built by the group of V.P. Chebotayev at the Institute of Laser Physics in Novosibirsk and was calibrated at the PTB in Braunschweig in a direct comparison to the Cs atomic clock with the help of the PTB frequency chain [6]. The result was (88376181599670$\pm$160) Hz with a relative uncertainty of $1.8 \cdot 10^{-12}$. In order to transport the accuracy of the HeNe/CH_4 to the 1S-2S frequency measurement, an additional reference frequency at the 8th harmonic (near 424 nm) is synthesized in three steps of second harmonic generation (Fig. 2, left side). To provide enough power for the nonlinear processes that are not very efficient in the optical part of the spectrum, we use additional lasers before each step of second harmonic generation. All these so called "transfer oscillators" are phase locked relative to their predecessors with the help of electronic servo loops. The output power of the HeNe/CH_4 standard is only 0.5 mW to avoid power broadening of the CH_4 resonance. A second HeNe laser with an output power of 20 mW is phase locked relative to the standard and half of its power is used to generate the second harmonic in a $AgGaSe_2$ crystal. At the second harmonic a NaCl:OH color-center laser provides an output power of 500 mW. The second harmonic of the color-center lasers radiation is generated in a $LiIO_3$ crystal. The laser diode at the 4th harmonic of the standard (848 nm) has an output power of 50 mW. A $KNbO_3$ crystal generates the second harmonic at 424 nm, which is the violet reference for the 1S-2S measurement. To determine the frequency of the dye laser, that is operating close to the 7th harmonic of the HeNe/CH_4, we generate the sum frequency of its blue light with the second half of the HeNe lasers radiation (10 mW) in a $LiNbO_3$ crystal. The sum frequency produced near the 8th harmonic of the HeNe/CH_4 is then compared to the violet reference by counting their radio-frequency beat note generated on a fast photodetector.

The frequency ratio of 1:28 between the CH_4 transition and the 1S-2S frequency does not hold exactly: the HeNe/CH_4 is operating at a frequency 300 GHz too high. Therefore a difference frequency Δf=2.1 THz has to be bridged at the 7 th harmonic of the HeNe/CH_4 between 617 THz (486 nm) and 619 THz (484 nm) (Fig. 2, right side). To determine Δf, we use different longitudinal modes of the

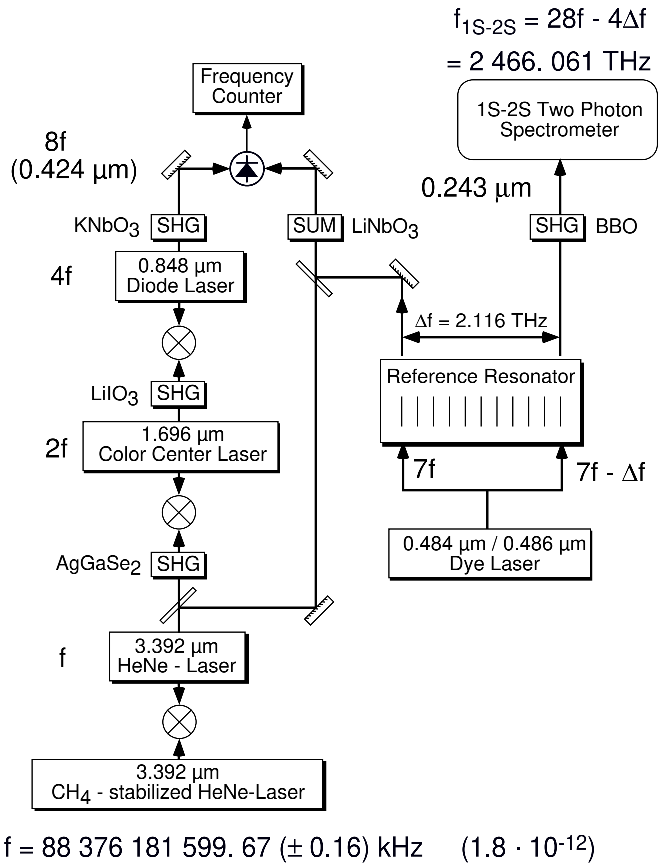

Figure 2: The frequency chain.

passive Fabry-Perot resonator, which is used to stabilize the dye laser. With the help of a second dye laser and an electro-optical modulator at 84 GHz we could calibrate the mode spacing of the resonator between the 7 th harmonic of the HeNe/CH_4 (619 THz) and 1/4 th of the 1S-2S transition frequency (617 THz) with an accuracy of better than 1 Hz [8].

Our result [1] for the hyperfine corrected frequency

$$f_{1S-2S} = 2466061413.182\,(45)\,\mathrm{MHz}\,, \tag{2}$$

is 18 times more accurate than the best [9] of the previous measurements. From our result for f_{1S-2S} and the most recent determination of the 1S-Lamb shift (see below and ref.[2]), we deduced a value of the Rydberg constant:

$$R_\infty = 109737,3156849(30)\,\mathrm{cm}^{-1}\,, \tag{3}$$

which is in good agreement with a recent result of a group at the ENS in Paris: R_∞=109737,3156834(24) cm^{-1} [10].

With a new fully phase coherent frequency measurement of the 1S-2S transition in atomic hydrogen and deuterium we expect to improve the accuracy of f_{1S-2S} again by more than one order of magnitude in the near future.

2.4 Measurement of the Lamb shift

In a second experiment the 1S-2S frequency is directly compared with that of 2S-4S via the combination:

$$E(4S-2S) - \frac{1}{4}E(2S-1S)\,. \tag{4}$$

For a frequency comparison of the 1S-2S and 2S-4S transitions, we lock the 1S-2S spectrometer to the maximum of the narrow 1S-2S signal. A small part of the infrared light provided by the Ti:Sapphire laser of the 2S-4S spectrometer is frequency doubled in a $KNbO_3$ crystal. The resulting blue light is mixed with the blue light from the dye laser locked to the 1S-2S transition on a fast photodiode,

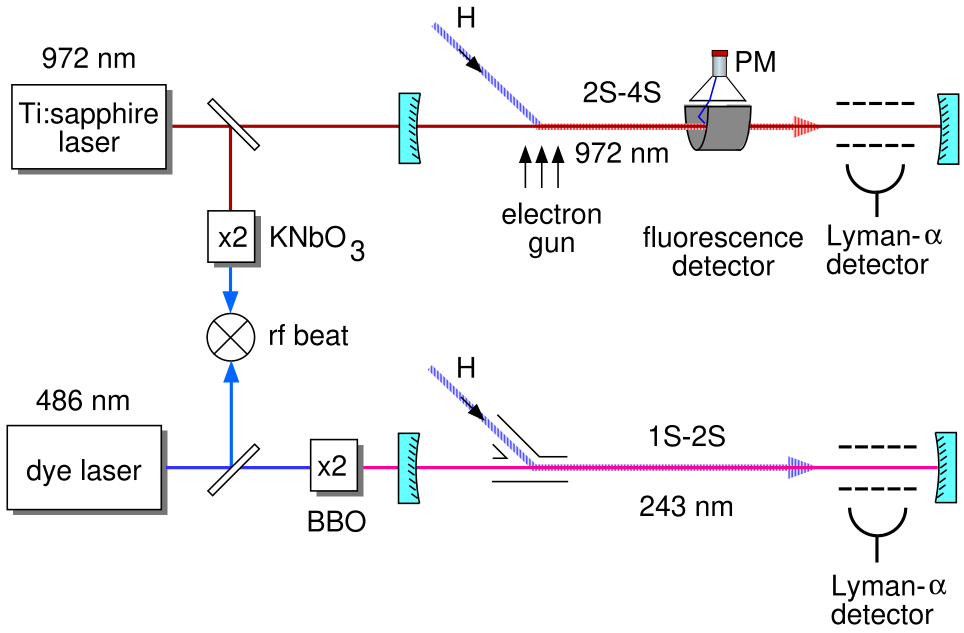

Figure 3: Frequency measurement of $E(4S-2S)-\frac{1}{4}E(2S-1S)$.

see Fig. 3. The frequency of the beat signal is measured both by a radio frequency counter and a spectrum analyzer locked to a rubidium standard. The Ti:sapphire laser is scanned over the 2S-4S resonance and the signal of both the metastable and the fluorescence detector is recorded versus the beat frequency. After averaging several such spectra, the obtained 2S-4S resonance lineshape is fitted with a theoretical model to extract the center frequency. In this way we obtained the value [2]:

$$L(4S-2S)-\frac{1}{4}L(2S-1S)=868\,631(10)\,\mathrm{kHz}\,. \tag{5}$$

From this combination the 1S Lamb shift for hydrogen can be derived using the experimental value for the smaller 2S-2P Lamb shift and the theoretical values for the 2P and 4S Lamb shifts shifts which are small and well known. Our result is

$$L_{1S}=8172.874(60)\,\mathrm{MHz}\,. \tag{6}$$

This value is in good agreement with a more recent measurement of D. Berkeland, E. Hinds and M. Boshier at Yale [11] obtained by a $1S-2S/2S-4P$ comparison $L(1S)=8172.827(51)$ MHz. A further measurement based on a comparison of $1S-3S/2S-6S$ has recently been communicated by F. Biraben and coworkers.

In a new experiment we hope to increase the accuracy to about 1 kHz by using the optically excited slow metastable beam of the 1S-2S spectrometer for further excitation into 4S state. This would allow one to significantly improve the value for the 1S and 2S Lamb shifts and for the Rydberg constant using the following equations:

$$L(1S) = \frac{64}{7}\left(\left[L(4S-2S)-\frac{1}{4}\,L(2S-1S)\right]_{exp}-\left[L(4S)-\frac{5}{4}L(2S)+\frac{9}{64}L(1S)\right]_{theo}\right)\,, \tag{7}$$

$$L(2S) = \frac{8}{7}\left(\left[L(4S-2S)-\frac{1}{4}\,L(2S-1S)\right]_{exp}-\left[L(4S)-\frac{17}{8}L(2S)+\frac{1}{4}\,L(1S)\right]_{theo}\right)\,, \tag{8}$$

$$\frac{3}{4}\frac{\mu}{m}R_\infty = E(2S-1S)_{exp}+8\left(E(4S-2S)-\frac{1}{4}E(2S-1S)\right)_{exp}-\Delta_{theo}\,, \tag{9}$$

$$\Delta_{theo} = \Delta_{rm}+\Big[8\,L(4S)-9\,L(2S)+L(1S)\Big]_{theo}\,, \tag{10}$$

where Δ_{rm} is a relativistic and reduced mass (denoted by μ) correction of the energy levels involved in the determination of the Rydberg constant, see Eq.(19). The subscripts *exp* and *theo* denote the experimental and theoretical values respectively. The coefficients are chosen in such a way, that all terms that scale with the principal number like $1/n^3$ are automatically cancelled in the energy level combinations of the theoretical part *theo*. It means that the nuclear finite size effect and most of the QED corrections do not contribute to them in the leading orders. Therefore, these combinations can be determined much more reliably and precisely than the Lamb shift for separate states. For example for the noted combination in the Rydberg constant determination we obtain

$$[8\,L(4S) - 9\,L(2S) + L(1S)]_{theo} = -178\,832(5)\,\mathrm{kHz}, \tag{11}$$

where the error comes from the unknown state dependence of B_{61} coefficient and is estimated as half of the known B_{62} contribution. S. Karshenboim [12] has first pointed out that the determination of the 1S Lamb shift could be significantly improved when the theoretical predictions for the $L(1S) - 8L(2S)$ difference are used, for which the $1/n^3$ terms cancel out. The above formulas will help to fully exploit the future high accuracy of the measurement of $L(4S - 2S) - 1/4\,L(2S - 1S)$. The similar idea has been already applied by M. Eides *et al.* in [27]. Since there is a new improved measurement of the electron-proton mass ratio by Van Dyck [14], the Rydberg constant as determined from (9) will be improved by an order of magnitude, after the new direct frequency measurement of the 1S-2S transition is performed. It will also be very interesting to compare the 2S Lamb shift derived from $L(4S - 2S) - 1/4\,L(2S - 1S)$ with the results obtained from Lundeen-Pipkin [15], Hagley-Pipkin [16] and Palchikov et al. [13], and thus to verify the different experimental methods.

2.5 Measurement of the hydrogen–deuterium isotope shift

In a third experiment we have measured the isotope shift of the 1S-2S transition of hydrogen and deuterium

$$\Delta_{\mathrm{ISO}} = E(2S - 1S)_{\mathrm{D}} - E(2S - 1S)_{\mathrm{H}}. \tag{12}$$

To overcome the limitations of former indirect measurements relative to an intermediate tellurium standard [9], we directly bridged the large frequency gap between the two resonances with a novel electro-optic phase modulator [8]. The light of a second dye laser (laser 2), stabilized similarly to the laser of the spectrometer, is sent through a nonlinear $LiTaO_3$-crystal inside the focus of an open millimeter-wave Fabry-Perot cavity. The standing millimeter-wave in this cavity modulates the index of refraction for the laser light inside the crystal. The light is guided through the crystal in a zig-zag path by multiple internal total reflections. In this way we achieve phase matching of the optical and millimeter-waves and a modulation index of about 5 % [8]. The millimeter-wave oscillator near 84 GHz is phase-locked to a rubidium frequency standard with an accuracy of better than 10^{-10}. The sideband spacing is twice the modulation frequency Ω,

$$2\Omega = (167347764.14 \pm 0.02)\ \mathrm{kHz}. \tag{13}$$

To move these sideband frequency markers near the hydrogen and deuterium resonances, the modulated laser carrier is tuned midway in between the resonance frequencies. While the first laser excites the 1S-2S transition of hydrogen or deuterium, the small residual beat frequencies Δn_D and Δn_H with the sidebands of the reference laser are recorded with a fast photodiode, followed by a spectrum analyzer. The spectrometer laser is alternatively stabilized to the 1S-2S resonances of hydrogen (hyperfine level $F = 1$) and deuterium (hyperfine level $F = 3/2$, $m_F = \pm 3/2$), while the beat note between laser 1 and the sidebands of laser 2 is recorded (Fig. 4). The frequency difference between the two-photon resonances at 243 nm is then given by:

$$\Delta_{exp} = 2(2\Omega + \Delta n_D - \Delta n_H), \tag{14}$$

where the factor of 2 arises from the frequency doubling of the 486 nm light. Because we cannot excite both resonances at the same time, and the reference resonator frequency of laser 2 is slowly drifting (approx. 15 Hz/s), the frequency marks are also drifting. To correct for this effect, we record the drifts of both beat frequencies with time. The drift of $\Delta n_D(t)$ is fitted with a polynomial of fourth order. The difference between measured $\Delta n_H(t)$ and interpolated $\Delta n_D(t)$ at the same times is constant within the measurement accuracy. The mean value has an uncertainty of 5 kHz due to the interpolation procedure described above. We correct for the hyperfine structure to obtain the line centroids. Our final result is

$$\Delta_{\mathrm{ISO}} = 670\ 994\ 337(22)\ \mathrm{kHz}\,, \tag{15}$$

which is in good agreement with the last measurement at Oxford [9], $\Delta_{\mathrm{ISO}} = 670\ 994.\ 33(64)$ MHz, but a factor of 25 more accurate.

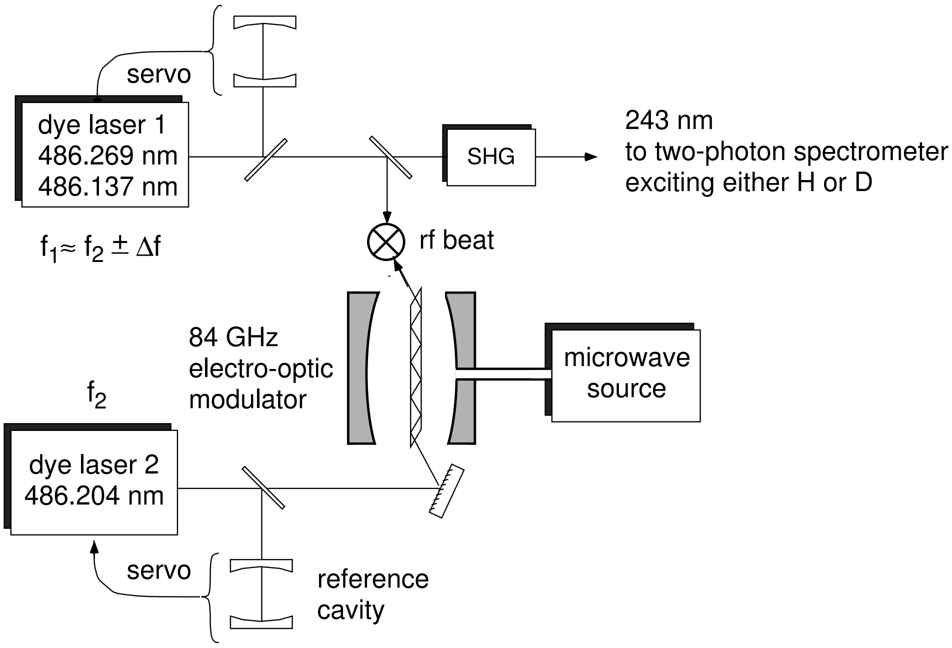

Figure 4: Frequency measurement of the hydrogen-deuterium isotope shift.

3 Theory of the hydrogen energy levels

Our goal is to present here an updated complete collection of known corrections to hydrogen energy levels including that, recently calculated. We concentrate mainly on S-states since these states are involved in our experiments. We base in this paper on the excellent review given by Sapirstein and Yennie in [4].

The hydrogen energy levels as given by Bohr $E = -\frac{m\,\alpha^2}{2\,n^2}$ do not exactly agree with the measured values. The most significant correction of order α^2 is due to relativistic effects described by the Dirac equation. One derives from this equation the following expression for electron energy levels in the Coulomb potential,

$$\begin{aligned} E(n,j) &= m\,f(n,j)\,, \\ f(n,j) &= \left(1+\frac{(Z\,\alpha)^2}{\left[n-j-\frac{1}{2}+\sqrt{(j+\frac{1}{2})^2-(Z\,\alpha)^2}\right]^2}\right)^{-\frac{1}{2}}\,, \end{aligned} \tag{16}$$

where n is the principal number, m is the mass of the electron, Z is the number of protons in the nucleus, α the fine structure constant, and j is the total angular momentum of the electron. In order to determine the energy levels with an accuracy comparable to Lamb shift experiments, one has to take into account the radiative and recoil corrections. The radiative corrections are due to the electron self-interaction, i.e. photon emission and immediate reabsorption and due to the vacuum polarization The recoil corrections are due to movement of the nucleus. Each photon exchange between the electron and the proton is accociated with a change of the proton kinetic energy. In the nonrelativistic limit, the proton mass dependence is accounted for by the reduced mass of the two-body system. The relativistic treatment is much more complicated and in general it is not even possible to write a two-body relativistic Hamiltonian. As a starting point one considers the approximated effective Hamiltonian, which is

$$H_{\mathrm{eff}} = \boldsymbol{\alpha}\cdot\mathbf{p}+\beta\,m+\frac{\mathbf{p}^2}{2M}+V_{\mathrm{eff}}\,, \tag{17}$$

$$V_{\mathrm{eff}} = -\frac{\alpha}{r}\left[1+\frac{1}{M}\left(\delta^{ij}+\frac{r^i\,r^j}{r^2}\right)\,p^i\,\alpha^j\right] \tag{18}$$

where α^i are the Dirac matrices , m and M are the electron and the nuclear mass respectively.

For simplicity we set $Z = 1$ since we are dealing with hydrogen. Apart from the Dirac factor this Hamiltonian contains the Breit interaction $V_{\rm eff}$ and the kinetic energy of the nucleus. The expression for the energy (not taking into account the hyperfine structure), that is valid up to order α^4 but gives the precise mass dependence is [17, 4]:

$$E = m + M + \mu\,[f(n,j) - 1] - \frac{\mu^2}{2\,(M+m)}\,[f(n,j)-1]^2 + \frac{\alpha^4\,\mu^3}{2\,n^3\,M^2}\left(\frac{1}{j+\frac{1}{2}} - \frac{1}{l+\frac{1}{2}}\right)(1-\delta_{l0})\,, \quad (19)$$

The remaining recoil corrections in higher order require separate treatment and will be described later. The Lamb shift is defined as the energy correction beyond the first four terms in the above formula.

The main contribution to the hydrogen Lamb shift is electron one-loop self-energy described by

$$\Delta E = e^2 \int \frac{d^4k}{(2\pi)^4 i}\,\frac{g_{\mu\nu}}{k^2}\,\langle\overline{\psi}|\gamma^\mu \frac{1}{\not p - \not k + \frac{\alpha}{r}\gamma^0 - m}\gamma^\nu|\psi\rangle - \langle\delta m\rangle\,, \quad (20)$$

and is represented by the Feynman graph on Fig. 5: Its evaluation has a rich history and in the last

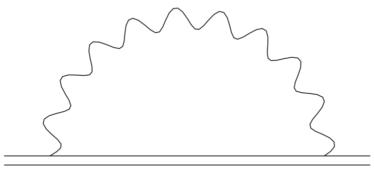

Figure 5: Electron self-energy diagram

years a significant progress has been made [18, 19]. There are mainly two complementary methods: the numerical one and the analytical one. The numerical method [20] is based on the decomposition of the Dirac-Coulomb Green function into partial waves. In the analytical method [21] one expands the expression (20) in α and calculates subsequently all the coefficients up to the order of interest. Both methods have some advantages and disadvantages. The direct numerical calculation for Z=1, (i.e. hydrogen) is extremely difficult, and so far the calculation has been done only for larger Z (Z=5,10, and so on). In the analytical calculation the coefficients in the α expansion are known precisely, but one always faces the estimation of uncalculated higher order terms. In fact these terms could also be obtained from the numerical integration data by extraction of the analytically known lower order terms and extrapolation to Z=1. Since we are here interested in the S-states, we limit the attention to this case. The coefficients in the analytical expansion are defined by:

$$\Delta E = \frac{m\,\alpha\,(Z\,\alpha)^4}{\pi\,n^3}\,F\,, \quad (21)$$

$$\begin{aligned} F &= A_{40} + A_{41}\,\ln\big[(Z\,\alpha)^{-2}\big] + A_{50}\,Z\,\alpha + \\ &\quad (Z\,\alpha)^2\,\big\{A_{60} + A_{61}\,\ln\big[(Z\,\alpha)^{-2}\big] + A_{62}\,\ln^2\big[(Z\,\alpha)^{-2}\big]\big\} + (Z\,\alpha)^3\,G \end{aligned} \quad (22)$$

where G incorporates all the higher order terms. The values for the electron self-energy for S-states are given in the following list:

$$\begin{aligned} A_{40}(n) &= \frac{10}{9} - \frac{4}{3}k_0(n) \\ \ln k_0(1) &= 2.9841285557655\,, \\ \ln k_0(2) &= 2.8117698931205\,, \\ \ln k_0(4) &= 2.7498118405\,, \\ A_{41} &= \frac{4}{3}\,, \\ A_{50} &= 4\pi\left(\frac{139}{128} - \frac{\ln(2)}{2}\right)\,, \\ A_{62} &= -1\,, \\ A_{61}(1) &= \frac{28}{3}\,\ln(2) - \frac{21}{20}\,, \end{aligned}$$

$$
\begin{aligned}
A_{61}(2) &= \frac{16}{3}\,\ln(2) + \frac{67}{30}\,, \\
A_{61}(4) &= \frac{4}{3}\,\ln(2) + \frac{391}{80}\,, \\
A_{60}(1) &= -30.92890\,, \\
A_{60}(2) &= -31.84047\,.
\end{aligned}
\tag{23}
$$

where $\ln k_0(n)$ denotes the Bethe logarithms [4]. Most of these data are taken from the comprehensive review of Sapirstein and Yennie in [4]. We have added the 4S state and the A_{60} coefficients for 1S and 2S states calculated by (K.P.) in [19]. The value for the A_{61} coefficient for the 4S state is taken from the review by Drake in [22].

$$
\begin{aligned}
A_{60}(4) &= -31.5(4)\,, \\
G(n) &= G'(n) + 2\,\pi\,\ln(Z\,\alpha)^{-2}\,, \\
G'(1) &= 26.9(5)\,, \\
G'(2) &= 29.8(10)\,, \\
G'(4) &= 27.2\,.
\end{aligned}
\tag{24}
$$

The term $A_{60}(4)$ and the remaining higher order terms summarized by G are calculated by extrapolation of numerical integration data obtained by P. Mohr [18, 23]. We have found it convenient for the extrapolation to subtract out a large $2\,\pi\,\ln(Z\,\alpha)^{-2}$ term. In this way one significantly decreases the dependence on $(Z\,\alpha)$. The extrapolation plots for $G'(1)$ and $G'(2)$ are presented on Fig. 6. We do not accociate an error to $G'(4)$, because it is already contained in $A_{60}(4)$.

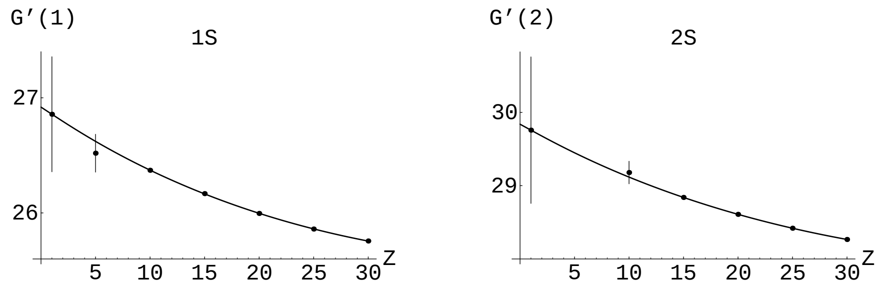

Figure 6: Extrapolation plots for 1S and 2S states. For most of the points the errors bars are inside the drawn size of the dots. The quoted values for Z=1 are the results of these extrapolations.

The next largest contribution to the Lamb shift is the one-loop vacuum polarization. It is given by the formula:

$$
\Delta E_{VP} \;=\; \int d^3\mathbf{x}_1 \int d^3\mathbf{x}_2\, \phi^{+}(\mathbf{x}_1)\,\phi(\mathbf{x}_1)\,\frac{\alpha}{|\mathbf{x}_1-\mathbf{x}_2|}(-i)\,\cdot \mathrm{Tr}\left[\gamma_0\, S_F(\mathbf{x}_2,\mathbf{x}_2,t=0)\right]\,,
\tag{25}
$$

where S_F is the Dirac-Coulomb propagator. This contribution is represented by the diagram shown in Fig. 7.

The calculation is done by expansion in α. The results are [4]:

$$
\begin{aligned}
A_{40} &= -\frac{4}{15}\,, \\
A_{50} &= -\frac{5\,\pi}{48}\,, \\
A_{61} &= -\frac{2}{15}\,,
\end{aligned}
$$

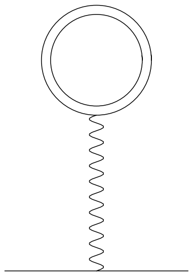

Figure 7: Vacuum polarization diagram

$$
\begin{aligned}
A_{60}(1) &= \frac{4}{15}\ln(2) - \frac{1289}{1575} + \left(\frac{19}{45} - \frac{\pi^2}{27}\right), \\
A_{60}(2) &= -\frac{743}{900} + \left(\frac{19}{45} - \frac{\pi^2}{27}\right), \\
A_{60}(4) &= -\frac{4}{15}\ln(2) - \frac{5363}{8400} + \left(\frac{19}{45} - \frac{\pi^2}{27}\right). \qquad (26)
\end{aligned}
$$

We did not find the coefficient $A_{60}(4)$ for the vacuum polarization in the literature, thus we have calculated it analytically. The unknown higher order terms are expected to contribute few kHz for the 1S state.

Further QED corrections are due to the two-loop diagrams. So far there is no complete direct numerical calculation of this correction. We therefore present the result of a calculation based on expansion in $Z\,\alpha$,

$$
\Delta E = \frac{m\,\alpha^2\,(Z\,\alpha)^4}{\pi^2\,n^3}\,\{B_{40} + Z\,\alpha\,B_{50} + (Z\,\alpha)^2[B_{63}\,\ln^3(Z\,\alpha)^{-2} + B_{62}\,\ln^2(Z\,\alpha)^{-2} + \ldots]\}\,. \qquad (27)
$$

The leading order term B_{40} is determined only by the electron form factors F_1' and F_2 at $q^2 = 0$ and the two-loop vacuum polarization [24],

$$
B_{40} = -\frac{2179}{648} - \frac{10\,\pi^2}{27} + \frac{3\,\pi^2\,\log(2)}{2} - \frac{9\,\zeta(3)}{4} = 0.538941 \qquad (28)
$$

The evaluation of the next to leading order term B_{50} was completed by one of us (K.P.), with the surprisingly large result

$$
B_{50} = -21.4(1)\,. \qquad (29)
$$

One class of the diagrams, that gives the largest contribution to B_{50}, is shown in Fig. 8. Recently M. Eides and coworkers [26, 27] have also finished the evaluation of this correction, and obtain a more accurate result which converted to our notation is

$$
B_{50} = -21.556(3) \qquad (30)
$$

in agreement with (29). Our value presented previously in the literature in [25] was slightly less accurate. In the meantime (K.P.) has improved and checked this result by an independent numerical integration. The problem in this calculation lies in the fact that every separate diagram is strongly divergent in the infrared, and only the complete sum is finite. Although, in some special gauges these diagrams could be finite, the corresponding expression is then much more complicated. Some details of this calculation and the checking methods are presented in the Appendix. It has been discovered by S. Karshenboim [28] that higher order terms could be also significant, because they are enhanced by powers of $\ln(Z\,\alpha)^{-2}$. His result for the coefficient B_{63} is $B_{63} = -\frac{8}{27}$ what gives about -3.6 kHz for 2S state. We will not include it in the theoretical value for the Lamb shift until other corrections of this order are known. For the evaluation of the Lamb shift combinations in (7), (8) and (10) the state dependent part of B_{62} could be significant. The expression

$$
B_{62} = \frac{16}{9}\left(\psi(n) + \frac{1}{4\,n^2} - \frac{1}{n} - \ln(n) + C\right), \qquad (31)
$$

where C is a n independent constant and ψ is a logarithmic derivative of Euler gamma function, was obtained in [12]. It contributes by about 10 kHz to the Lamb shift combination (10).

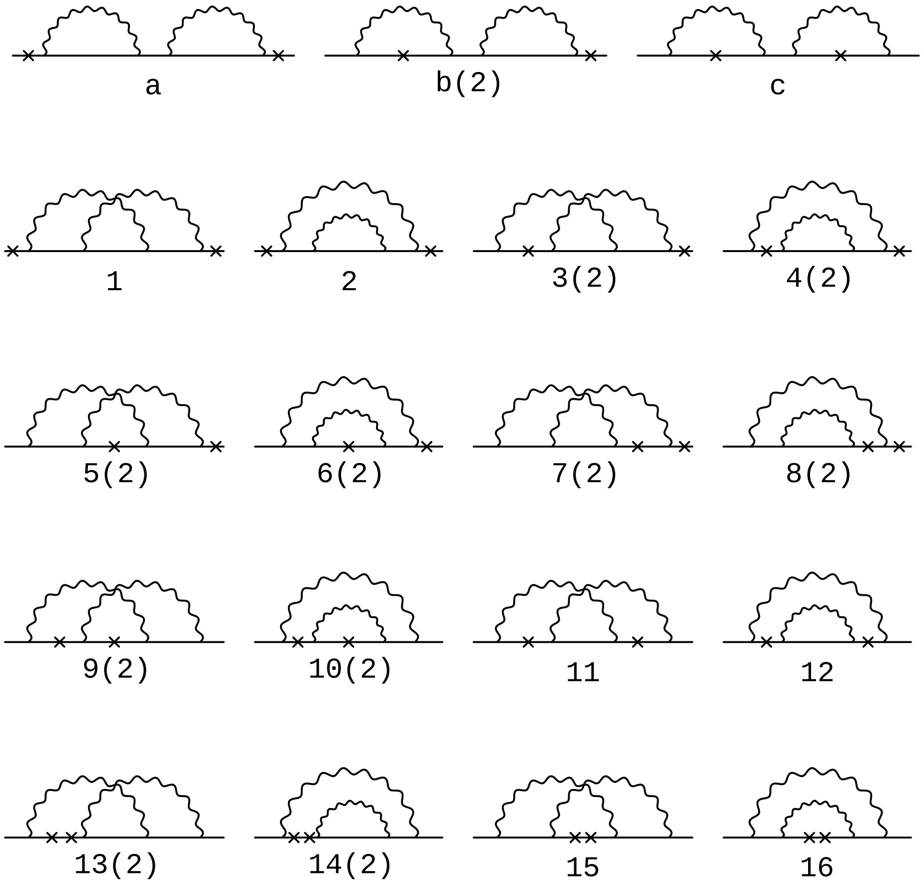

Figure 8: Two-loop diagrams; the cross denotes the insertion of the Coulomb vertex.

At this point we have a complete set of known corrections in the limit of infinite nuclear mass. The additional recoil corrections, due to movement of the nucleus, beyond formula (19) are conventionally divided into pure and radiative recoil corrections. The pure recoil corrections include all diagrams with the exchange of photons between electron and nucleus, neglecting the self-interaction, see Fig. 9:

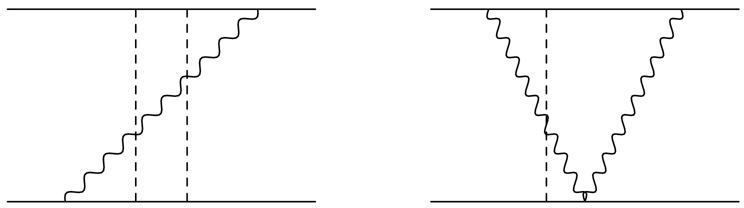

Figure 9: Some diagrams for pure recoil corrections; waved and dashed lines denote the transverse and Coulomb photon respectively

The exact mass dependence of the pure recoil correction in α^5 order was worked out in [29] using the Bethe–Salpeter formalism.

$$\Delta E = \frac{\mu^3}{m\,M}\frac{\alpha^5}{\pi\,n^3} \quad \Bigg\{ \quad \frac{2}{3}\,\delta_{l0}\,\ln(\frac{1}{\alpha}) - \frac{8}{3}\,\ln k_0(n,l) - \frac{1}{9}\,\delta_{l0} - \frac{7}{3}\,a_n$$
$$-\frac{2}{M^2-m^2}\,\delta_{l0}\,\left[M^2\,\ln\left(\frac{m}{\mu}\right) - m^2\,\ln\left(\frac{M}{\mu}\right)\right]\Bigg\}\,, \qquad (32)$$

where

$$a_n = -2\left(\ln(\frac{2}{n}) + (1+\frac{1}{2}+\ldots+\frac{1}{n}) + 1 - \frac{1}{2\,n}\right)\,\delta_{l0} + \frac{1-\delta_{l0}}{l\,(l+1)\,(2\,l+1)}\,, \tag{33}$$

and μ denotes the reduced mass and $\ln k_0(n)$ the Bethe logarithm.

In order α^6 the m/M correction has been calculated in [30] using the effective potential method. It has been found that this calculation contains some errors. Khriplovich and coworkers [31] calculated the exact mass dependence of the logarithmic term for the case of arbitrary masses and found that the $\log(\alpha)$ term should be absent. A recent calculation of one of us (K.P.) together with H. Grotch [32] gives the complete result for the pure recoil corrections in order $(Z\,\alpha)^6$,

$$\Delta E(nS) = \frac{m^2}{M}\,\frac{(Z\,\alpha)^6}{n^3}\left(4\,\ln(2) - \frac{7}{2}\right)\,. \tag{34}$$

The radiative recoil corrections include the diagrams where a photon is emitted and absorbed by the same particle, or the photon propagator is modified by the fermion loop. It has been checked in

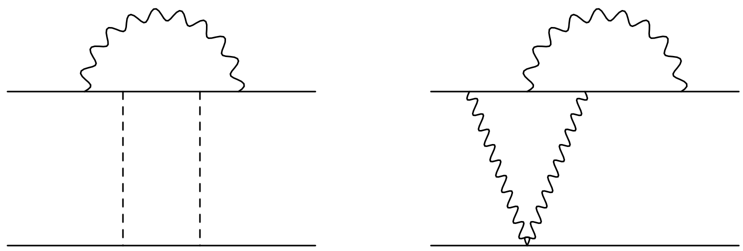

Figure 10: Some diagrams for the radiative recoil corrections.

[33, 4] that for S-states most of these corrections could be incorporated by multiplying the radiative corrections (electron self-energy, vacuum polarization and two-loop corrections) by a factor $(\mu/m)^3$, which comes from the modification of the wave function at the origin, and changing the argument of $\ln(Z\,\alpha)^{-2}$ to $\ln\left(\frac{m}{\mu}(Z\,\alpha)^{-2}\right)$ which is twice the logarithm of the ratio of binding energy and electron rest energy. These replacement rules give an exact expression for the recoil correction in order $\alpha\,(Z\,\alpha)^4$, but there are some corrections in order $\alpha\,(Z\,\alpha)^5$ which are not yet incorporated. Some example diagrams are presented in Fig. 10. This radiative recoil correction has originally been calculated in [33]

$$\Delta E = -\frac{\alpha\,(Z\,\alpha)^5\,m^2}{M\,n^3}\,1.988(4)\,, \tag{35}$$

but it has been recently recalculated in [34] with the result:

$$\Delta E = -\frac{\alpha\,(Z\,\alpha)^5\,m^2}{M\,n^3}\,1.36449\,. \tag{36}$$

Due to different method used in [34] the origin of the discrepancy has not yet been found. A small difference is due to inclusion of vacuum polarization terms, but the greatest difference comes from the so called pole contribution.

There are some conceptional problems with the proton self-energy correction. For a point-like proton it would be

$$\Delta E = \frac{\alpha^5\,\mu^3}{\pi\,n^3\,M^2}\left[\left(\frac{10}{9} + \frac{4}{3}\,\ln\frac{M}{\mu\,\alpha^2}\right)\,\delta_{l0} - \frac{4}{3}\,\ln k_0(n,l)\right] \tag{37}$$

For a finite size proton some corrections in the above are counted twice because they are already incorporated in the proton charge radius. This problem has been considered in [34]. The conclusion is that only the logarithmic term should be excluded from the nuclear finite size contribution. Therefore the complete nuclear size and self-energy correction for S-states and any nuclear charge has the form

$$\Delta E = \frac{2}{3\,n^3}\,(Z\,\alpha)^4\,\mu^3\langle r^2\rangle + \frac{4\,\mu^3}{3\,\pi\,n^3\,M^2}\,(Z^2\,\alpha)\,(Z\,\alpha)^4\left[\ln\left(\frac{M}{\mu\,(Z\,\alpha)^2}\right) - \ln k_0(n)\right]\,, \tag{38}$$

where $\langle r^2 \rangle$ denotes the nuclear charge radius. The additional correction in the expression above beyond the finite size effect gives 4.6 kHz for the 1S state in hydrogen.

There are some additional corrections that are specific for deuterium. The binding energy of the deuteron 2.2 MeV is comparable to the electron mass, giving rise to a small polarizability correction. We have estimated this correction [35] using the square well potential for the proton-neutron interaction,

$$\Delta E = -m\,\alpha\,\phi(0)^2\,\alpha_d\,\left(\frac{19}{6} + 5\,\ln(2\,\bar{E})\right)\,. \tag{39}$$

where $\bar{E} = 4.915$ MeV, and $\alpha_d = 0.635\,\text{fm}^3$ is a deuteron polarizability. This correction gives -22(2) kHz for 1S state in deuterium. A more precise results using different models has later been obtained by J. Martorell *et al.* [36] ΔE = 22.09(24) kHz, and Leidemann *et al.* [37] ΔE = -21.5(3) kHz, which agree with our estimation.

Since the deuteron has spin 1 the Zitterbewegung term in the $1/c$ expansion is absent. It means that there is an additional recoil correction beyond Eq. (19) for deuterium [38],

$$\Delta E = -\frac{1}{2}\,\frac{\mu^3}{M^2}\,\frac{(Z\,\alpha)^4}{n^3}\,\delta_{l0} \tag{40}$$

It contributes -13 kHz for the 1S state in deuterium. Both corrections are significant for a determination of the deuteron radius from the hydrogen-deuterium isotope shift [3].

4 Conclusions

The theoretical predictions for the Lamb shifts of hydrogen energy levels, using a proton *rms* radius $r_p = 0.862(12)$ fm [39] are:

$$\begin{aligned}
L(1S) &= 8172802(32)(24)\,\text{kHz}\,, && (41)\\
L(2S) &= 1045003(4)(3)\,\text{kHz}\,, && (42)\\
L(4S) &= 131675.2(5)(4)\,\text{kHz}\,, && (43)\\
L(4S-2S) - \frac{1}{4}L(2S-1S) &= 868622(4)(3)\,\text{kHz}\,, && (44)\\
L(2S-2P) &= 1057839(4)(4)\,\text{kHz}\,, && (45)
\end{aligned}$$

where the first error comes from proton radius and the second from the estimation of higher order two-loop corrections and three loop contribution. For the evaluation of the 2P Lamb shift we used data given in [4], except for $G_{SE}(2P)$. For this higher order term we perform an extrapolation of improved data obtained by P. Mohr [18] with the result: $A_{60}(2P) = -0.96(7)$, $A_{70}(2P) = 2.6$. The coefficient $A_{71}(2P)$ is exactly zero.

The older proton radius $r_p = 0.805(11)$ [40] will give a result which is 18 kHz smaller for the $2S$ Lamb shift and 16 kHz smaller for the combined Lamb shift. Comparing the theoretical predictions with the experimental results:

$$\begin{aligned}
L(2S_{1/2} - 2P_{1/2}) &= 1\,057\,845(9)\,\text{kHz}\ [15] && (46)\\
L(2S_{1/2} - 2P_{1/2}) &= 1\,057\,839(12)\,\text{kHz}\ [16]\,, && (47)\\
L(4S-2S) - \frac{1}{4}\,L(2S-1S) &= 868631(10)\,\text{kHz}\ [2]\,. && (48)
\end{aligned}$$

a satisfactory agreement is found if the larger value for the proton radius is used.

Although, the recently calculated two-loop correction leads to agreement of the hydrogen experimental results with the theoretical predictions based on the newer proton radius, a strong disagreement appears for the He$^+$ Lamb shift, as first noted by M. Boshier [41]. The theory predicts:

$$L_{He}(2S-2P) = 14\,041.33(18)\,\text{MHz}\,, \tag{49}$$

while the experimental result of Wijngaarden et al. [42] is

$$L_{He}(2S-2P) = 14\,042.52(16)\,\text{MHz}\,. \tag{50}$$

These results are presented in Fig. 11. The strong disagreement between He^+ experiment and the-

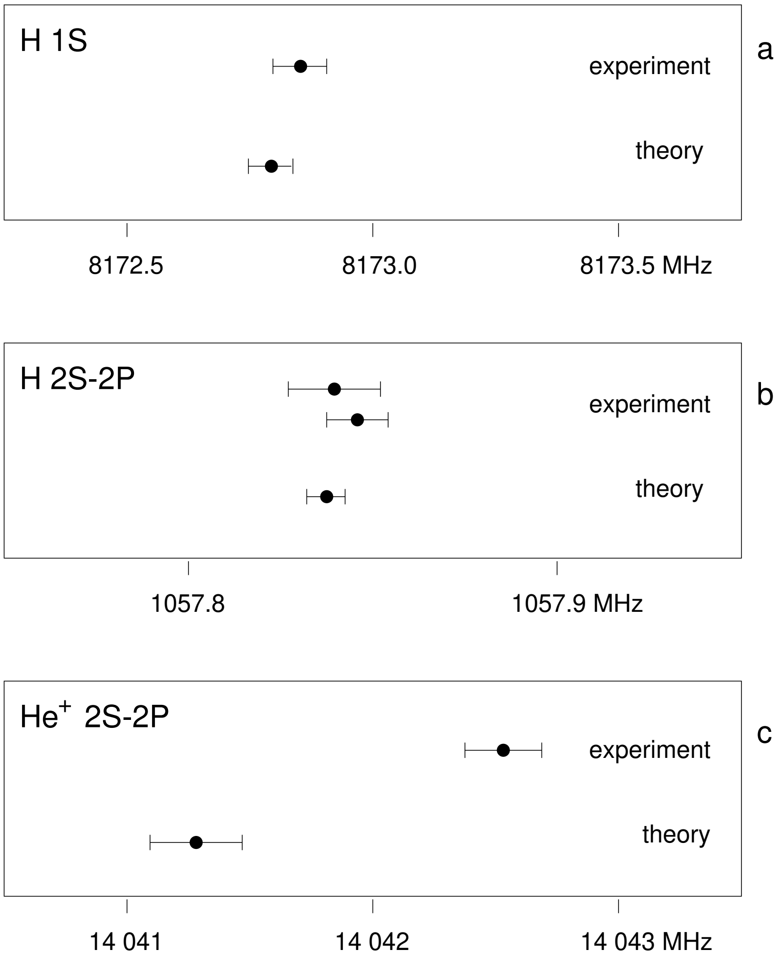

Figure 11: The hydrogen and helium$^+$ Lamb shift, experimental value in 'a' is from [2], in 'b' from [16] and [15], in 'c' from [42]

oretical predictions clearly requires further investigation. In fact the theoretical side has now been confirmed by an independent calculation of M. Eides et. al. [27] and the experimental side will be checked by a measurement of Boshier and Hinds [11], where the hydrogen 1S-2S transition will be compared to the He$^+$ 2S-4S transition.

An even more critical test of QED using L(2S-4S)-1/4 L(1S-2S) is currently limited by the uncertainty in the proton radius which, for example, leads to an error of 4 kHz for the 2S Lamb shift, compared to the predicted accuracy of 1 kHz of the planned measurement of the combined Lamb shift (48). A considerably improved test of QED based on hydrogen requires a more precise determination of the proton charge radius, which should be possible by a Lamb shift measurement in muonic hydrogen. Such an experiment is currently planned at PSI [43].

The most significant uncertainties of the theoretical Lamb shifts and H-D isotope shift are due to

- unknown complete two-loop correction of order $\alpha^2\,(Z\,\alpha)^6$,
- three-loop contribution of order $\alpha^3\,(Z\,\alpha)^4$,
- pure and radiative recoil corrections of order $\frac{m^2}{M}\,\alpha^7\,\ln^2(\alpha)^{-2}$,

which are estimated to be about 3 kHz for 2S state. The evaluation of these corrections becomes now the main problem in the theory of the hydrogen Lamb shift. A precise determination of the state dependent part of B_{61} is important for a possible determination of the Rydberg constant from equation (9) and higher order recoil corrections are significant for the isotope shifts. We have left unevaluated the vacuum polarization correction caused by heavier particles and for example ρ meson contribution to photon formfactor. They could be simply included as a nuclear finite size effect.

From the measurement of the hydrogen-deuterium isotope shift we could determine the value of the deuteron matter radius. Summing up all the reduced mass and Lamb shift contributions, but excluding the nuclear finite size contribution we obtain a theoretical value of

$$[E_D(2S-1S) - E_H(2S-1S)]' = 670999572(2)(4)\,\mathrm{kHz}\,, \tag{51}$$

where the first error comes from the proton-electron mass ratio and the second is the estimate of unknown recoil corrections in order $\frac{m^2}{M}\alpha^7$, which are enhanced by the factor $\ln^2(\alpha)^{-2}$. In this calculation we used the following values for the proton-electron [14] and deuteron-proton [45] mass ratios

$$\frac{m_p}{m_e} = 1836.1526646(58)\,, \tag{52}$$

$$\frac{m_d}{m_p} = 1.9990075013(14)\,. \tag{53}$$

The difference

$$\Delta E = 5235(22)\,\mathrm{kHz} \tag{54}$$

between the theoretical value (51) and experimental value (15) is caused by the nuclear finite size effect

$$\Delta E = \frac{2}{3\,n^3}\,(Z\,\alpha)^4\,\mu^3\langle r^2\rangle\,. \tag{55}$$

Using this equation we obtain for the difference of the deuteron-proton charge square radii,

$$r_d^2 - r_p^2 = 3.822(16)\,\mathrm{fm}^2\,, \tag{56}$$

where r_d and r_p respectively denote the deuteron and proton *rms* nuclear charge radii. The error of 0.016 fm^2 in (56) is dominated by the 22 kHz error in the measurement of the hydrogen-deuterium isotope shift. The deuteron matter radius r_m is defined by the formula [46]

$$r_d^2 = r_p^2 + r_m^2 + r_n^2 + \frac{3}{4}\,\frac{1}{{m_p}^2}\,, \tag{57}$$

where $r_n^2 = -0.1192\,\mathrm{fm}^2$ is the neutron charge radius. From the experimental isotope shift of 1S-2S, we obtain a deuteron matter radius r_m

$$r_m = 1.977(4)\,\mathrm{fm}\,. \tag{58}$$

This value disagrees with the matter radius obtained from electron scattering experiments (see [46] and references therein)

$$r_m = 1.953(3)\,\mathrm{fm}\,, \tag{59}$$

but is in better agreement with that calculated using the effective nucleon-nucleon interaction potential [47],

$$r_m = 1.968(1)\,\mathrm{fm}\,. \tag{60}$$

These results suggest that the interpretation of low energy electron–deuteron scattering data may require an additional analysis to obtain the correct deuteron charge radius.

The present theory of hydrogen-like systems shows that one perfectly understands all the QED effects, which in principle could be calculated up to any order (except for the nuclear structure corrections). The difficulties are technical, due to complicated expressions exploding in the higher order calculations. Also, there is still no unified treatment of two-body systems in the sense that higher orders terms can not be calculated automatically. Usually one has to perform some approximation, i.e. expansions in α, before the expression can be calculated. This is the trickiest part of all these calculations. There exist several methods for different types of corrections, see [44] and [19] for example, which exploit the fact that different photon gauges are appropriate for the low and high energy regions. It allows for the elimination of spurious singularities at the earlier stage of calculations. But still there is no method for the bound state problems where all corrections are treated in an unified way. One example for these difficulties is the orthopositronium decay rate, where the calculation of the correction in order α^2 is still not completed.

Appendix

In this appendix we briefly describe the calculation of the most difficult class of two-loop binding contributions that was performed by one of us (K.P.) [25], and consists of the diagrams shown in Fig. 8. We also explain how this method has been tested.

There are three momenta involved in the expression generated from the Feynman diagrams: two photon four-momenta k_1 and k_2 and the three-dimensional momentum $\mathbf{p}$ transfered through the Coulomb vertices. The correction to the energy described by the coefficient $F = B_{50}$ can be written as

$$\begin{aligned} \Delta E &= \left(\frac{\alpha}{\pi}\right)^2 \frac{(Z\,\alpha)^5}{n^3}\,F\,, \\ F &= \int \frac{d^3\,p}{\pi^2} \int \frac{d^4\,k_2}{\pi^2} \int \frac{d^4\,k_1}{\pi^2}\; \frac{1}{4\,p^4}\Big(f(p,k_1,k_2) - f(0,k_1,k_2)\Big)\,. \end{aligned} \tag{61}$$

The problem in the calculation lies in the fact that the integration in p is divergent for separate diagrams. The evaluation proceeds as follows. Assuming that the k_1 and k_2 integrations are done, F could be rewritten to the form

$$F = \frac{1}{4}\int \frac{d^3p}{\pi^2}\frac{1}{p^4}\left(f(p^2) - f(0)\right)\,, \tag{62}$$

where f is an analytical function with a branch cut along the negative axis. From the Cauchy theorem we have

$$f(p^2) = -\int_0^\infty d(q^2)\frac{1}{p^2+q^2}f^A(q^2)\,,$$

$$f(p^2) - f(0) = p^2\int_0^\infty d(q^2)\frac{1}{q^2\,(p^2+q^2)}f^A(q^2)\,, \tag{63}$$

$$F = \int_0^\infty dq\,\frac{f^A(q^2)}{q^2}\,. \tag{64}$$

In this way the integral is converted to a form suitable for the further analytical treatment. It is calculated analytically the expansion of $f^A(q^2)$ up to q^{10}. The first terms in this expansion are

$$f^A(q^2) = -\frac{32}{27}q^2 + \frac{104}{9}q^2\,\ln(q^2) + \ldots \tag{65}$$

The integral (64) with respect to q from 0 to $q^2 = \frac{1}{2}$ is performed using this analytical expansion, while for $q^2 > \frac{1}{2}$ the integral is evaluated numerically using the Feynman parameter approach. For the final value we obtained

$$B_{50} = -21.4(1)\,. \tag{66}$$

To check this result several tests were performed. The first logarithmic term in the q^2 expansion of f^A gives the most significant contribution to the B_{50}. It was independly calculated by S. Karshenboim in Yennie gauge, and by us in the Feynman and Coulomb gauge. The next test was the comparison of the numerical part with the analytic expansion at $q^2 = \frac{1}{2}$. The further and the most significant test was done using the fact that for a similar integral

$$f(0) = -\int_0^\infty d(q^2)\frac{1}{q^2}f^A(q^2)\,, \tag{67}$$

the analytical result is known. It is given by the on shell vertex functions, similar to the leading two-loop contribution (diagrams without closed fermion loop).

$$f(0) = 32F_1'(0) + 8F_2(0)\,. \tag{68}$$

Using the values for the appropriate diagrams [48] the analytical value is

$$f(0) = -\frac{163}{9} - \frac{85\,\pi^2}{27} + 12\,\pi^2\,\ln(2) - 18\,\zeta(3) = 11.27\,. \tag{69}$$

The combined analytical-numerical code gives

$$f(0) = 11.14(12)\,, \tag{70}$$

at photon mass $\mu^2 = 0.4\cdot 10^{-4}$.

The improved value for B_{50} is presented. It is in agreement with the previous one [25], and was obtained by recalculation of the numerical part.

Acknowledgments

We acknowledge the valuable contributions of V.P. Chebotayev, F. Schmidt-Kaler, R. Wynands, T. Andreae, C. Zimmermann and M. Prevedelli. The experimental part of this work has been supported in part by the Deutsche Forschungsgemeinschaft and within the frame of an EU science program cooperation, contract No. SCI*-CT92-0816..

References

[1] T. Andreae, W. König, R. Wynands, D. Leibfried, F. Schmidt-Kaler, C. Zimmermann, D. Meschede, and T. W. Hänsch, Phys. Rev. Lett., **69**, 1923 (1992).

[2] M. Weitz, A. Huber, F. Schmidt-Kaler, D. Leibfried, and T.W. Hänsch, Phys. Rev. Lett. **72**, 328 (1994); M. Weitz, A. Huber, F. Schmidt-Kaler, D. Leibfried, W. Vassen, C. Zimmermann, K. Pachucki, T.W. Hänsch, L. Julien, and F. Biraben, Phys. Rev. A, *in press*

[3] F. Schmidt-Kaler, D. Leibfried, M. Weitz, and T. W. Hänsch, Phys. Rev. Lett. **70**, 2261 (1993).

[4] J. R. Sapirstein and D. R. Yennie, in *Quantum Electrodynamics*, Editor T. Kinoshita, World Scientific (1990).

[5] F.Schmidt-Kaler, D. Leibfried, S. Seel, C. Zimmermann, W. König, M. Weitz, and T.W. Hänsch, Phys. Rev. A **51**, 2789 (1995).

[6] C.O. Weiss, G. Kramer, B. Lipphardt, E. Garcia, IEEE J. Quantum Electron. **QE-24**, 1970 (1988).

[7] B. Dahmani, L. Hollberg, and R. Drullinger, Opt. Lett. **12**, 876 (1987).

[8] D. Leibfried, F. Schmidt-Kaler, M. Weitz, and T.W. Hänsch, Appl. Phys. B **56**. 65 (1993).

[9] M.G. Boshier, P.G.E. Baird, C.J. Foot, E.A. Hinds, M.D. Plimmer, D.N. Stacey, J.B. Swan, D.A. Tate, D.M. Warrington, G.K. Woodgate, Phys. Rev. A **40**, 6169 (1989).

[10] F. Nez, M.D. Plimmer, S. Bourzeix, L. Julien, F. Biraben, R. Felder, Y. Milleroux, and P. de Natale, Europhys. Lett **24**, 635 (1993).

[11] D.J. Berkeland, E.A. Hinds and M. Boshier, Phy. Rev. Lett. **75** 2470 (1995).

[12] S.G. Karshenboim, JETP, *in press.*

[13] V. G. Pal'chikov, Yu. L. Sokolov, and V. P. Yakovlev, JETP Lett. **38**, 418 (1983).

[14] R.S. van Dyck, Jr., *et al.*, *private communication.*

[15] S. R. Lundeen, F. M. Pipkin, Phys. Rev. Lett. **46**, 232 (1981).

[16] E.W. Hagley and F.M. Pipkin, Phys.Rev.Lett. **72**, 1172, (1994).

[17] W.A. Barker and F.N. Glover, Phys. Rev. **99**, 317 (1955).

[18] P. J. Mohr, Phys. Rev. A **46**,4421, (1992).

[19] K. Pachucki, Phys. Rev. A, **46** 648, (1992), Ann. Phys. (N.Y.), **226** 1, (1993).

[20] P. J. Mohr, Ann. Phys. (N.Y) **88**, 26, 52 (1974).

[21] G. W. Erickson and D. R. Yennie, Ann. Phys. (N.Y) **35**, 271, 447 (1965).

[22] G.W.F. Drake, Adv. At. Mol. Opt. Phys. **31**, 1 (1993).

[23] P. J. Mohr and Y.-K. Kim, Phys. Rev. A **45**, 2727 (1992).

[24] R. Barbieri, J. A. Mignaco, and E. Remiddi, Nuovo Cim. Lett. **3**, 588 (1970)
B. E. Lautrup, A. Peterman, and E. de Rafael, Phys. Lett. B **31** , 577 (1970).

[25] K. Pachucki, Phys. Rev. A, **48**, 2609 (1993); Phys. Rev. Lett. **72**, 3154 (1994).

[26] M.I. Eides and H. Grotch, Phys. Lett. B **301**, 127 (1993), Phy. Lett. B **308**, 389 (1993) M. Eides, H. Grotch, and P. Pebler, Phys. Rev. A **50**, 144 (1994).

[27] M. Eides and V. Shelyuto, Phys. Rev. A **52**, 954 (1995), and references therein.

[28] S. G. Karshenboim, JETP **76**, 541 (1993).

[29] E. E. Salpeter, Phys. Rev. **87**, 328 (1952), G.W. Erickson, J. Phys. Chem. Ref. Data **6**, 833 (1977).

[30] M. Doncheski, H. Grotch and G.W. Erickson, Phys. Rev. A **43**, 2125 (1991).

[31] I. B. Khriplovich, A. I. Milstein and A. S. Yelkhovsky, Phys. Scrip. **T46**, 252 (1993), R. N. Fell, I. B. Khriplovich, A. I. Milstein and A. S. Yelkhovsky, Phys. Lett. A **181**, 172 (1993).

[32] K. Pachucki and H. Grotch, Phys. Rev. A **51**, 1854 (1995).

[33] G. Bhatt and H. Grotch, Ann. Phys. (NY) **178**,1 (1987).

[34] K. Pachucki, Phys. Rev. A **52**, 1079 (1995).

[35] K. Pachucki, D. Leibfried, and T.W. Hänsch, Phys. Rev. A **48**, R1 (1993). K. Pachucki, M. Weitz, and T.W. Hänsch, Phys. Rev. A. **49**, 2255 (1994).

[36] J. Martorell, D.W. Sprung, and D.C. Zheng, Phys. Rev. C **51**, 1127 (1995).

[37] W. Leidemann and R. Rosenfelder, Phys. Rev. C **51**, 427 (1995).

[38] K. Pachucki and S. Karshenboim, J. Phys. B **28**, L221 (1995).

[39] G. G. Simon, C. Schmidt, F. Borkowski, and V. H. Walther, Nucl. Phys. A **333**, 381 (1980).

[40] L. N. Hand, D. J. Miller, and R. Wilson, Rev. Mod. Phys. **35**, 335 (1963).

[41] M. Boshier, *private communication.*

[42] A. van Wijngaarden, J. Kwela, and G.W.F. Drake, Phys. Rev. A **43**, 3325 (1991).

[43] D. Taqqu, Paul Scherrer Institut, Villingen Suisse, *private communication.*

[44] T. Kinoshita and P. Lepage, in Quantum Electrodynamics, edited by T. Kinoshita, (World Scientific, Singapore, 1990), p. 560.

[45] G. Audi and A.H. Waspra, Nucl. Phys. A **565**, 1 (1993).

[46] S. Klarsfeld *et al*, Nucl. Phys. **A456**, 373 (1986).

[47] J. L. Friar, G.L. Payne, V.G.J. Stoks, and J.J. de Swart, Phys. Lett. B**311**, 4 (1993).

[48] R. Barbieri, J.A. Mignaco, and E. Remiddi, Nuovo Cim. **11A**, 824 (1972).